Inverse Problems in Science and Engineering

Publication details, including instructions for authors and subscription information:
http://www.tandfonline.com/loi/gipe20

Topology optimization in electromagnetic casting via quadratic programming

Alfredo Canelas [a] & Jean R. Roche [b]

[a] Facultad de Ingeniería , Instituto de Estructuras y Transporte, UDELAR , Montevideo , Uruguay

[b] CNRS, INRIA, Institut Elie Cartan de Lorraine, Université de Lorraine , Nancy , France

Published online: 18 Apr 2013.

To cite this article: Alfredo Canelas & Jean R. Roche , Inverse Problems in Science and Engineering (2013): Topology optimization in electromagnetic casting via quadratic programming, Inverse Problems in Science and Engineering, DOI: 10.1080/17415977.2013.788173

To link to this article: http://dx.doi.org/10.1080/17415977.2013.788173

Inverse Problems in Science and Engineering, 2013
http://dx.doi.org/10.1080/17415977.2013.788173

Taylor & Francis
Taylor & Francis Group

Topology optimization in electromagnetic casting via quadratic programming

Alfredo Canelas[a*] and Jean R. Roche[b]

[a] *Facultad de Ingeniería, Instituto de Estructuras y Transporte, UDELAR, Montevideo, Uruguay;*
[b] *CNRS, INRIA, Institut Elie Cartan de Lorraine, Université de Lorraine, Nancy, France*

(*Received 21 November 2012; final version received 18 March 2013*)

A new optimization method is proposed for solving an inverse problem concerning the shape and topology of the inductors used in the electromagnetic casting technique of the metallurgical industry. The method is based on an sparse convex quadratic programming version of a recently proposed topology optimization formulation of the inverse electromagnetic casting problem. Regular 0–1 solutions are found by adding to the original Kohn–Vogelius objective function an appropriate penalty term that preserves the quadratic programming structure of the problem, allowing the use of efficient interior-point algorithms. Results for some numerical examples are presented, showing that the technique proposed is effective and can successfully find inductors of optimal shape and topology.

Keywords: inverse problem; topology optimization; electromagnetic casting; quadratic programming; interior-point methods

AMS Subject Classifications: 49Q10; 90C90; 90C51; 65K10; 65R32

1. Introduction

This paper concerns the numerical solution of an inverse problem regarding electromagnetic casting (EMC) of molten metals. The EMC is an industrial technique that allows for contactless heating, shaping and controlling of chemically aggressive hot melts. It makes use of the repulsive forces that an electromagnetic field produces on the surface of a mass of liquid metal. Under suitable assumptions, the equilibrium configurations are described by a set equations expressing an equilibrium relation on the liquid metal surface between the electromagnetic pressure and the surface tension forces. The equilibrium relation involves the curvature of the surface and the solution of an elliptic exterior boundary value problem.

The inverse EMC problem considered in this paper consists of determining the electric currents that induce the exterior magnetic field for which the liquid metal takes on a given desired shape. In previous works, we studied the inverse EMC problem in the case that the inductors are single solid-core wires of negligible cross-sectional area, and the more realistic case where they are made of a set of bounded insulated strands.[1–3] In both cases the number of inductors was fixed in advance. In a later article, we overcame this limitation and looked for optimal configurations of inductors considering a topology optimization formulation based on the Kohn–Vogelius criterion, which was solved by means of a topology optimization technique based on the topological derivative concept.[4]

*Corresponding author. Email: acanelas@fing.edu.uy

In the present paper, we consider the topology optimization formulation proposed in [4] and state a simultaneous design and optimization (SAND) formulation of the inverse EMC problem. In this formulation, we add a penalty term to the Kohn–Vogelius criterion with the purpose of obtaining regular 0–1 solutions. We show that the discrete version of the penalized SAND formulation is a convex quadratic programming problem that can be efficiently solved by using interior-point optimization algorithms. In addition to the interior-point algorithm, a simple variable mesh approach is proposed to further reduce the computational costs of solution.

The remaining contents of this paper are organized as follows. Section 2 briefly describes the mathematical model of the EMC problem. Section 3 introduces the inverse EMC problem and describes the penalized SAND topology optimization formulation and the variable mesh approach. Some numerical examples of two-dimensional exterior and interior EMC problems are studied in Section 4. Finally, the concluding remarks are given in Section 5.

2. The mathematical model of the EMC problem

In several EMC applications, the electromagnetic field is induced by an alternating current, and the resulting Lorentz forces cause hydrodynamics effects in the liquid metal, see [5–12]. The penetration of the electromagnetic field into the metal is governed by an induction equation depending on the fluid velocity and the magnetic diffusivity. By increasing the frequency, while keeping the field scale fixed, the magnetic Reynolds number becomes small, and Sneyd and Moffatt [13,14] have shown that we can neglect the velocity term in the calculation of the induced field. Hence, we are faced with a standard problem of field penetration into a solid conductor. This results in an exponential decay of the field inside the conductor which is known as the skin effect. Therefore, for a sufficient high frequency, the Lorentz forces are concentrated on a thin layer on the metal surface, and the penetration of the field inside the metal can be neglected.

The simplified model of the EMC problem studied here concerns the case of a vertical column of liquid metal falling down into an electromagnetic field created by vertical inductors. We consider the quasi-static model and assume that the frequency of the imposed electric current is very high, so that we rely on the skin effect. Moreover, we assume that a stationary horizontal section is reached so that the two-dimensional model is valid. The equilibrium of the system is ensured by the static balance on the surface of the metal between the surface tension and the electromagnetic forces. This problem and other similar ones have been considered by several authors, we refer the reader to the papers [5,6,15–20] for the physical analysis of the simplifying assumptions of the model.

Let $\Omega \subset \mathbb{R}^2$ be the exterior of the domain ω occupied by the cross-section of the metal column, which is assumed closed, simply connected and with a non-void interior. Under these assumptions, the equilibrium surface Γ of the molten metal column is characterized by the following Equations [20–24]:

$$\nabla \times \boldsymbol{B} = \mu_0 \boldsymbol{J} \quad \text{in } \Omega, \tag{1}$$

$$\nabla \cdot \boldsymbol{B} = 0 \quad \text{in } \Omega, \tag{2}$$

$$\boldsymbol{B} \cdot \nu = 0 \quad \text{on } \Gamma, \tag{3}$$

$$\|\boldsymbol{B}(x)\| = O(\|x\|^{-1}) \quad \text{as } \|x\| \to \infty \text{ in } \Omega, \tag{4}$$

$$\frac{1}{2\mu_0}\|\boldsymbol{B}\|^2 + \sigma\mathcal{C} = p_0 \qquad \text{on } \Gamma. \tag{5}$$

Here, the fields $\boldsymbol{J} = (0, 0, j_0)$ and $\boldsymbol{B} = (B_1, B_2, 0)$ represent the mean square values of the electric current density vector and the total magnetic field, respectively. The constant μ_0 is the vacuum permeability, ν is the unit normal vector to the boundary Γ and $\|\cdot\|$ denotes the Euclidean norm. In (5) $\mathcal{C}$ is the curvature of Γ seen from the metal, σ is the surface tension of the liquid and the constant p_0 is an unknown of the problem. Physically, p_0 represents the difference between the internal and external pressures. Equations (1)–(5) correspond to the *exterior* EMC problem. In the *interior* EMC problem Ω is assumed open, bounded an simply connected, and (4) is discarded. In both cases, we assume that j_0 has a compact support in Ω and that the total electric current is zero:

$$\int_\Omega j_0\, dx = 0. \tag{6}$$

In the exterior EMC problem we assume that the cross-sectional area of the liquid metal column is known and equal to S_0:

$$\int_\omega dx = S_0, \tag{7}$$

while, in the case of the interior problem, Ω replaces ω in (7).

Equations (1)–(6), with the function j_0 compactly supported in Ω, imply the existence of the flux function $\varphi : \Omega \to \mathbb{R}$ such that $\boldsymbol{B} = (\frac{\partial\varphi}{\partial x_2}, -\frac{\partial\varphi}{\partial x_1}, 0)$. Then, the boundary value problem regarding the inverse EMC problem in terms of the flux function is:

$$\begin{cases} -\Delta\varphi = \mu_0 j_0 & \text{in } \Omega\,, \\ \varphi = 0 & \text{on } \Gamma\,, \\ \varphi(x) = c + o(1) & \text{as } \|x\| \to \infty\,, \end{cases} \tag{8}$$

where the constant c is the value at infinity of the solution φ in the case of the exterior problem, which is also an unknown of (8) [1,2,4], while the condition at infinity is not considered in the interior EMC problem. Equivalent formulations of the condition at infinity are $\varphi(x) = O(1)$ and $\varphi(x) = c + O(\|x\|^{-1})$.[25] The form used in (8) is convenient in the development of numerical methods of solution.

Problem (8) has unique solutions $\varphi \in W_0^1(\Omega)$ and $c \in \mathbb{R}$ [25,26], where $W_0^1(\Omega)$ is defined as:

$$W_0^1(\Omega) = \{u :\ \beta\, u \in L^2(\Omega) \text{ and } \nabla u \in L^2(\Omega)\}\,, \tag{9}$$

with $\beta(x) = [\sqrt{1 + \|x\|^2}\, \log(2 + \|x\|^2)]^{-1}$ in the exterior EMC problem and $\beta = 1$ in the interior one. The equilibrium of the liquid metal surface in terms of the flux function is:

$$\frac{1}{2\mu_0}\left|\frac{\partial\varphi}{\partial n}\right|^2 + \sigma\mathcal{C} = p_0 \quad \text{on } \Gamma\,. \tag{10}$$

In the direct EMC problem the electric current density j_0 and the cross-sectional area S_0 are given, and one has to find the shape of ω satisfying (7) such that the flux

function φ solution to (8) satisfies also the equilibrium Equation (10) for a real constant p_0. Alternatively, the equilibrium shape can be found as a stationary state of a total energy functional under the constraint that the cross-sectional area is prescribed, see [16,17].

3. The inverse EMC problem

For clarity of exposition, we restrict the description of the inverse problem formulation to the case of the exterior EMC problem. The formulation of the interior problem is deduced following the same steps. The goal of the inverse problem is to find a distribution of electric current around the liquid metal column so that it attains a given target shape ω, limited by a smooth boundary Γ and with exterior Ω. Therefore, we have to determine the electric current density j_0 satisfying (6) such that the solution φ of (8) satisfies also the equilibrium Equation (10). Note the different role of the shape ω in the inverse problem: it is not an unknown, it is the data of the problem.

There are a few papers about the existence of exact solutions to the inverse problem, see [18,27]. Although these above-mentioned references constitute an important insight on the existence issue, we are also interested in obtaining approximate solutions in situations where the existence of solutions cannot be ensured. If the inverse problem has an exact solution, we say that the target shape is shapable, if it does not, we say that it is not shapable. Even considering a shapable shape, the inverse problem is inherently ill-posed: small variations of the liquid surface may cause dramatic variations in the solution j_0 of the inverse problem.[18,27] In addition, the uniqueness of the solution in terms of j_0 cannot be ensured.[4] Hence, we follow the approach proposed in [4], where the inverse problem is formulated as an optimization problem, in order to look for a solution (maybe just an approximate solution) minimizing an appropriate functional.

There are, however, some known facts about the exact solutions of the inverse problem that are of main importance in what follows. From (5) and (10), we realize that p_0 must satisfy

$$p_0 \geq \max_{\Gamma} \sigma \mathcal{C}\,, \tag{11}$$

to have the field $\|\boldsymbol{B}\|$ well determined on Γ by conditions (3) and (5).[4,18] In addition, (3) requires that Γ be an analytic curve, and the existence of j_0 satisfying (6) requires that $p_0 = \max_\Gamma \sigma\mathcal{C}$. In that case, the curvature $\mathcal{C}$ of a shapable domain ω must reach its maximum value at an even number of points.[18]

Given p_0 by the equality in (11), the equilibrium equation reads

$$\frac{\partial \varphi}{\partial n} = \varkappa\, \bar{p} \quad \text{on } \Gamma, \tag{12}$$

where $\bar{p} = \sqrt{2\mu_0(p_0 - \sigma\mathcal{C})}$, and $\varkappa = \pm 1$, with the changes of sign located at the points where the curvature of Γ is a global maximum. The two possible ways of defining $\varkappa$ lead to the same solution j_0 but with the opposite sign.[4] Therefore, we assume from now on that $\varkappa\,\bar{p}$ is a known function defined on Γ.

It is also possible to introduce some constraints in the position of the inductors to have realizable solutions. Considering a shapable ω, Henrot and Pierre [18] proved that a solution with the electric current concentrated on a closed curve located at a small enough distance of Γ can always be found.

3.1. *Problem Formulation*

The considerations made in Section 3 allow us to formulate the inverse problem as follows: for the target shape ω, limited by a smooth boundary Γ and with exterior Ω, determine an electric current density j_0 satisfying (6) with compact support $\mathrm{spt}(j_0) \subset \Theta$, where Θ is a given compact in Ω,[18] and a real constant c such that the system

$$\begin{cases} -\Delta\varphi = \mu_0 j_0 & \text{in } \Omega\,, \\ \varphi = 0 & \text{on } \Gamma\,, \\ \dfrac{\partial\varphi}{\partial n} = \varkappa\,\bar{p} & \text{on } \Gamma\,, \\ \varphi(x) = c + o(1) & \text{as } \|x\| \to \infty\,, \end{cases} \tag{13}$$

has a solution $\varphi \in W_0^1(\Omega)$. Therefore, a necessary condition for the existence of a solution to the inverse problem is the following [4]:

$$\int_\Gamma \varkappa\,\bar{p}\,ds = 0\,. \tag{14}$$

Let us introduce a shape functional based on the Kohn–Vogelius criterion, namely

$$J(\phi) = \frac{1}{2}\|\phi\|^2_{L^2(\Gamma)} = \frac{1}{2}\int_\Gamma \phi^2\,ds, \tag{15}$$

where the auxiliary function ϕ depends implicitly on j_0 and c by solving the following boundary value problem:

$$\begin{cases} -\Delta\phi = \mu_0 j_0 & \text{in } \Omega, \\ \dfrac{\partial\phi}{\partial n} = \varkappa\,\bar{p} & \text{on } \Gamma, \\ \phi(x) = c + o(1) & \text{as } \|x\| \to \infty\,. \end{cases} \tag{16}$$

Note that (16) has a unique solution in $W_0^1(\Omega)$ if and only if the compatibility condition (14) is satisfied.[25,28]

The approach proposed in [4] to deal with (13) is the following: determine the electric current density j_0 and the constant c such that the solution ϕ of (16) minimizes the shape functional (15). We note that the minimum of the shape functional (15) is attained when $\phi \equiv 0$ on Γ. This means that in this situation, from the well-posedness of problems (8) and (16), we have $\phi \equiv \varphi$ in Ω.

A SAND approach for the previous problem can be obtained considering j_0 and ϕ as independent variables of the optimization problem, and (16) as an equality constraint, see [1,2,29] and references therein given. Let $\psi(j_0)$ be the total absolute electric current function given by

$$\psi(j_0) = \|j_0\|_{L_1(\Omega)} = \int_\Omega |j_0|\,dx\,. \tag{17}$$

We propose the following penalized SAND formulation of the inverse EMC problem:

$$\begin{aligned} &\min_{j_0,\phi,c} \; J(\phi) + \rho\psi(j_0)\,, \\ &\text{s.t.} \quad \begin{cases} -\Delta\phi = \mu_0 j_0 & \text{in } \Omega, \\ \dfrac{\partial\phi}{\partial n} = \varkappa\,\bar{p} & \text{on } \Gamma, \\ \phi(x) = c + o(1) & \text{as } \|x\| \to \infty, \end{cases} \\ &\int_\Omega j_0\,dx = 0\,, \\ &|j_0| \le I, \end{aligned} \tag{18}$$

where I is a given bound for the electric current density, and $\rho\psi(j_0)$ acts as a penalty term depending on the penalty parameter ρ. Formulation (18) relaxes the one considered in [4], where j_0 was required to be a 0–1 solution, i.e. to satisfy $j_0(x) \in \{-I, 0, I\}$ at each $x \in \Omega$. However, we will show numerically that the addition of the penalty term produces three important beneficial effects on the solution: (i) it produces regularization of the solution, (ii) it penalizes solutions with a high total absolute electric current and (iii) it leads to 0–1 solutions in a natural manner, so avoiding intermediate values of j_0 in the set $(-I, 0) \cup (0, I)$. We will show also that in the discrete version, this penalty term preserves the quadratic programming structure of the original problem. This is very important and unusual in the topology optimization field, where the penalty approaches used to obtain 0–1 solutions, for example when using the Solid Isotropic Microstructure with Penalization method (SIMP),[30,31] usually lead to non-convex formulations with multiple suboptimal local minima.[32,33] We stress again that ω is the known target shape of the inverse problem, then we do not need to consider the area constraint (7) in the formulation. The main advantage of this approach is the absence of shape variables, which usually lead to highly non-linear and non-convex formulations. However, after solving (18), the equilibrium shape for the optimized inductors must be computed, and we have to check that it does not differ significantly from the target shape, see [1,2].

3.2. *The discrete convex quadratic programming formulation*

The solution to the inverse problem must consist of a simple configuration of inductors. In the discrete version of (18) we look for an electric current density distribution j_0 of the form:

$$j_0 = I \sum_{p=1}^{m} \alpha_p \chi_{\Theta_p}, \tag{19}$$

where $\alpha_p \in [-1, 1]$ for each $1 \le p \le m$, the cells Θ_p are fixed disjoint bounded domains satisfying $\Theta = \cup_{p=1}^{m} \Theta_p \subset \Omega$, and χ_{Θ_p} denotes the characteristic function of Θ_p. Note that the electric current density j_0 is uniform on each Θ_p. Inductors made of bundled insulated strands allow the implementation of good approximations to such kind of distribution, see [34] and references therein.

To deal with the exterior boundary value problem of (18), we rely on the following integral equation for the solution ϕ [25,28,35,36]:

$$c(\xi)\phi(\xi) + \int_\Gamma q^*\phi\,ds - \int_\Gamma u^*\varkappa\bar{p}\,ds = c + \int_\Omega u^*\mu_0 j_0(x)\,dx, \tag{20}$$

where u^* is the fundamental solution of the problem, $u^*(\xi, x) = -\log \|\xi - x\|/(2\pi)$, q^* is the normal derivative of u^*, the characteristic function $c(\xi) = 1$, for each interior point ξ and $c(\xi) = \Delta\theta/(2\pi)$, for each point $\xi \in \Gamma$, where $\Delta\theta$ is the angle, internal to Ω, formed by the right and left tangents to Γ at ξ. The first integral on the left-hand side of (20) must be understood in the Cauchy principal value sense.

The spatial discretization consists of approximating the boundary Γ into N linear elements Γ_j, $1 \leq j \leq N$. The functions ϕ and $\varkappa\bar{p}$ are approximated inside each element by piecewise linear polynomials in the form:

$$\phi(x) = \boldsymbol{N}(x)\boldsymbol{\phi}^{(j)}, \quad \varkappa(x)\bar{p}(x) = \boldsymbol{N}(x)\bar{\boldsymbol{p}}^{(j)}, \quad \text{in } \Gamma_j, \tag{21}$$

where $\boldsymbol{N} \in \mathbb{R}^{1\times 2}$ is the matrix of the linear interpolation functions and $\boldsymbol{\phi}^{(j)}$ and $\bar{\boldsymbol{p}}^{(j)}$ are the vectors that contain the nodal values corresponding to ϕ and $\varkappa\,\bar{p}$ in the element Γ_j. The collocation boundary element method,[35,36] builds a linear system imposing (20) at each node ξ_i of the boundary mesh:

$$c_i\boldsymbol{\phi}_i + \sum_{j=1}^{N} \boldsymbol{h}_{ij}\boldsymbol{\phi}^{(j)} - \sum_{j=1}^{N} \boldsymbol{g}_{ij}\boldsymbol{q}^{(j)} = c + \boldsymbol{A}_i\boldsymbol{\alpha}, \quad 1 \leq i \leq N, \tag{22}$$

where the element matrices $\boldsymbol{h}_{ij}$ and $\boldsymbol{g}_{ij}$ are:

$$\boldsymbol{h}_{ij} = \int_{\Gamma_j} q^*(\xi_i, x)\boldsymbol{N}(x)\,ds, \quad \boldsymbol{g}_{ij} = \int_{\Gamma_j} u^*(\xi_i, x)\boldsymbol{N}(x)\,ds, \tag{23}$$

$\boldsymbol{\alpha} \in \mathbb{R}^m$ is the vector with the values α_p and the matrix $\boldsymbol{A} \in \mathbb{R}^{N\times m}$ is given by:

$$\boldsymbol{A}_{ij} = \int_{\Theta_j} u^*(\xi_i, x) I\mu_0\,dx. \tag{24}$$

The linear system (22) can be expressed in matrix form as:

$$\boldsymbol{H}\boldsymbol{\phi} - \boldsymbol{G}\bar{\boldsymbol{p}} = c\boldsymbol{d} + \boldsymbol{A}\boldsymbol{\alpha}, \tag{25}$$

where $\boldsymbol{H} \in \mathbb{R}^{N\times N}$ is assembled from the values of c_i and $\boldsymbol{h}_{ij}$, $\boldsymbol{G} \in \mathbb{R}^{N\times N}$ is assembled from the values of matrices $\boldsymbol{g}_{ij}$, the vectors $\boldsymbol{\phi} \in \mathbb{R}^N$ and $\bar{\boldsymbol{p}} \in \mathbb{R}^N$ contain all the nodal variables corresponding to ϕ and $\varkappa\,\bar{p}$, respectively, and $\boldsymbol{d} \in \mathbb{R}^N$ is the vector with all components equal to one. In addition, we have

$$J(\phi) = \frac{1}{2}\int_{\Gamma} \phi^2\,ds = \frac{1}{2}\boldsymbol{\phi}^T\boldsymbol{M}\boldsymbol{\phi}, \tag{26}$$

$$\int_{\Omega} j_0\,ds = \boldsymbol{e}^T\boldsymbol{\alpha}, \quad \psi(j_0) = \int_{\Omega} |j_0|\,ds = \boldsymbol{e}^T|\boldsymbol{\alpha}|, \tag{27}$$

where the sparse matrix $\boldsymbol{M} \in \mathbb{R}^{N\times N}$ is obtained by integrating the interpolation functions and $\boldsymbol{e} \in \mathbb{R}^m$ is obtained from (19) and (27).

Finally, by defining the positive and negative parts $\boldsymbol{\alpha}^+ \in \mathbb{R}^m$, $\boldsymbol{\alpha}^- \in \mathbb{R}^m$ of $\boldsymbol{\alpha}$ by $\boldsymbol{\alpha}_p^+ = \max\{0, \boldsymbol{\alpha}_p\}$ and $\boldsymbol{\alpha}_p^- = \max\{0, -\boldsymbol{\alpha}_p\}$, we have $\boldsymbol{\alpha} = \boldsymbol{\alpha}^+ - \boldsymbol{\alpha}^-$, and $|\boldsymbol{\alpha}| = \boldsymbol{\alpha}^+ + \boldsymbol{\alpha}^-$. Therefore, from (25) and (26)–(27) we can formulate a discrete version of (18) as the following convex quadratic programming problem:

$$\begin{aligned} \min_{\boldsymbol{\alpha}^+,\boldsymbol{\alpha}^-,\boldsymbol{\phi},c} \quad & \tfrac{1}{2}\boldsymbol{\phi}^T \boldsymbol{M}\boldsymbol{\phi} + \rho \boldsymbol{e}^T \left(\boldsymbol{\alpha}^+ + \boldsymbol{\alpha}^-\right), \\ \text{s.t.} \quad & \boldsymbol{H}\boldsymbol{\phi} - \boldsymbol{G}\bar{\boldsymbol{p}} = c\boldsymbol{d} + \boldsymbol{A}\left(\boldsymbol{\alpha}^+ - \boldsymbol{\alpha}^-\right), \\ & \boldsymbol{e}^T \left(\boldsymbol{\alpha}^+ - \boldsymbol{\alpha}^-\right) = 0, \\ & 0 \leq \boldsymbol{\alpha}^+ \leq 1, \\ & 0 \leq \boldsymbol{\alpha}^- \leq 1. \end{aligned} \tag{28}$$

Note that the first N equality constraints are defined by the boundary element matrices $\boldsymbol{H}$, $\boldsymbol{G}$ and $\boldsymbol{A}$ that are full in the general case. However, if the number of cells is much larger than the number of boundary elements, i.e. if $m >> N$, then Problem (28) is sparse. The data of the problem are $\boldsymbol{M}$, ρ, $\boldsymbol{e}$, $\boldsymbol{H}$, $\boldsymbol{G}$, $\boldsymbol{d}$ and $\boldsymbol{A}$, where $\boldsymbol{H}$, $\boldsymbol{G}$ and $\boldsymbol{A}$ are obtained by Gaussian quadrature, and $\boldsymbol{M}$ and $\boldsymbol{e}$ are integrated analytically.

3.2.1. *A simple variable mesh approach*

Even though (28) is a sparse convex quadratic programming problem for which there are very efficient algorithms of solution for large-scale problems, the implementation of a variable mesh approach can reduce the computational costs of solution dramatically. As we will show in Section 4, the introduction of the penalty term leads to regular 0–1 solutions having large regions of constant electric current density, whose geometric representation can be improved by refining the mesh nearby their boundaries. Hence, the simple variable mesh approach proposed is the following: start with a coarse mesh, solve Problem (28) and refine the mesh subdividing those cells whose dimensionless electric current density α_p differs more than a specified tolerance of the corresponding value of any of the adjacent cells, i.e. we subdivide in four smaller cells, each cell Θ_p of the mesh having an adjacent cell Θ_q such that $|\alpha_p - \alpha_q| > \text{Tol}_\alpha$, where Tol_α is the chosen tolerance. In addition, for better representing the geometry of Θ, we also subdivide the cells adjacent to its boundary.

4. Numerical examples

To show the efficacy of the proposed approach we present results for five examples. In physically compatible units, we have set $\sigma = 1.0 \times 10^{-4}$ and $\mu_0 = 1.0$ for all the examples. When using the variable mesh approach, the value $\text{Tol}_\alpha = 1.0 \times 10^{-2}$ has been specified. To solve the finite dimensional convex quadratic problems, we have used the *quadprog* routine of the Optimization Toolbox™ of MATLAB®. The *interior-point-convex* option with TolFun $= 1.0 \times 10^{-18}$ has been considered. The numerical experiments have been carried out in a laptop PC with an Intel® Core™ i7 M620 2.67 GHz CPU and 6.0 GiB of RAM. For all the examples we give a contour plot of the optimized solution $I^{-1} j_0$, and represent the corresponding equilibrium shape together with the target shape.

The target shape of the first example is the same as the example 2 of [4]. It is the solution of a direct free-surface problem for a liquid metal column of cross-sectional area $S_0 = \pi$, with six distributed electric currents of density $I = 0.4$ as shown in Figure 1. Then, the six inductors constitute an optimal solution for the inverse problem. However, from the numerical point of view, this solution is not exactly optimal for the current formulation, since the approaches used to solve the direct and the inverse problems are different. For example, in the approach for the direct problem a weak formulation of the equilibrium equation was considered, see [1,2]. In addition, there is numerical evidence indicating that the solution to the inverse problem is not unique.[4] For these reasons, the optimized solutions are very

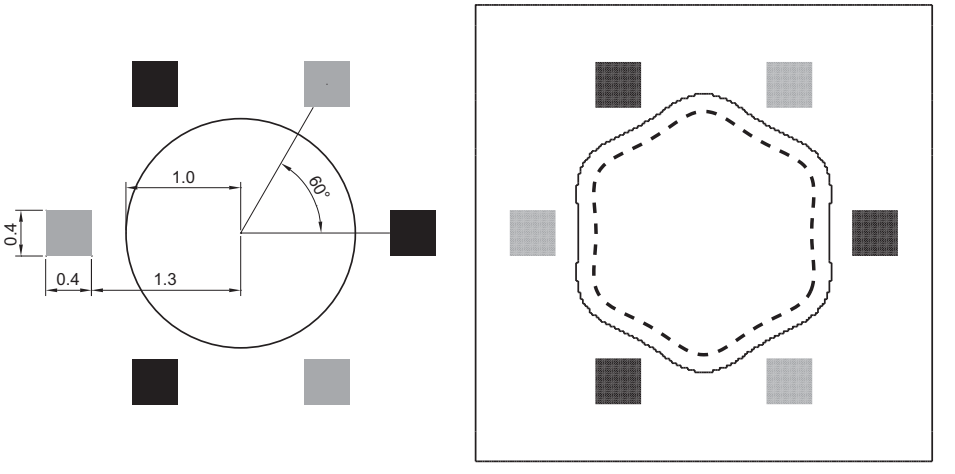

Figure 1. Example 1 – (a) initial configuration of the direct free-surface problem, (b) target shape of area $S_0 = \pi$. Black area: positive inductors, grey area: negative inductors, dashed line: target shape, thin solid line: boundary of the mesh of cells.

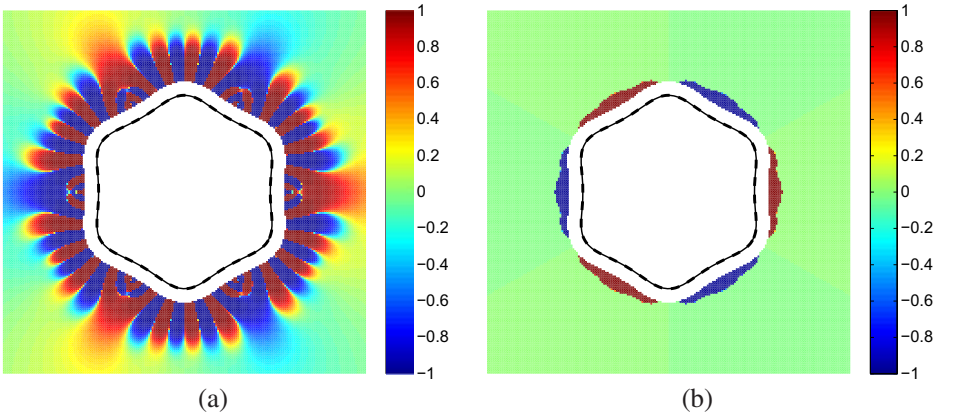

Figure 2. Example 1 – contour plot of $I^{-1} j_0$, (a) $\rho = 0$, (b) $\rho = 1 \times 10^{-7}$. Dashed line: target shape, thin solid line: equilibrium shape obtained for the optimized inductors.

different from the configuration given in Figure 1. Figure 2(a) shows the solution obtained for a penalty parameter $\rho = 0$ on a fixed mesh of cells of size 0.02. This solution has three main characteristics that are highly undesired for manufacturing purposes: first, it shows an irregular pattern with the electric current density varying from -1 to 1 in the region near the liquid metal. Second, it is not a 0–1 solution, since outside the region near the liquid metal, the values of α_p vary continuously in the range $[-1, 1]$. Third, the total absolute electric current $\psi(j_0)$ is high. Figure 2(b) shows the solution obtained for a penalty parameter $\rho = 1 \times 10^{-7}$. It is a regular 0–1 solution for the inverse EMC problem, i.e.

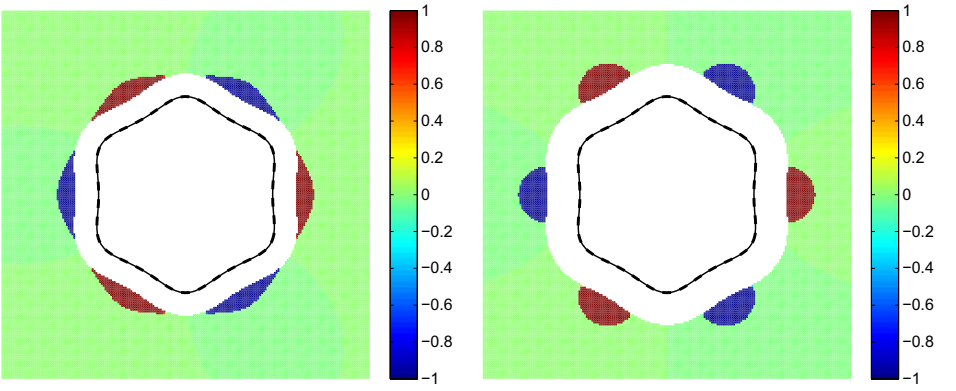

Figure 3. Example 1 – contour plot of $I^{-1} j_0$, (a) inductors located to a distance $d = 0.25$ from the liquid metal, (b) $d = 0.35$. Dashed line: target shape, thin solid line: equilibrium shape obtained for the optimized inductors.

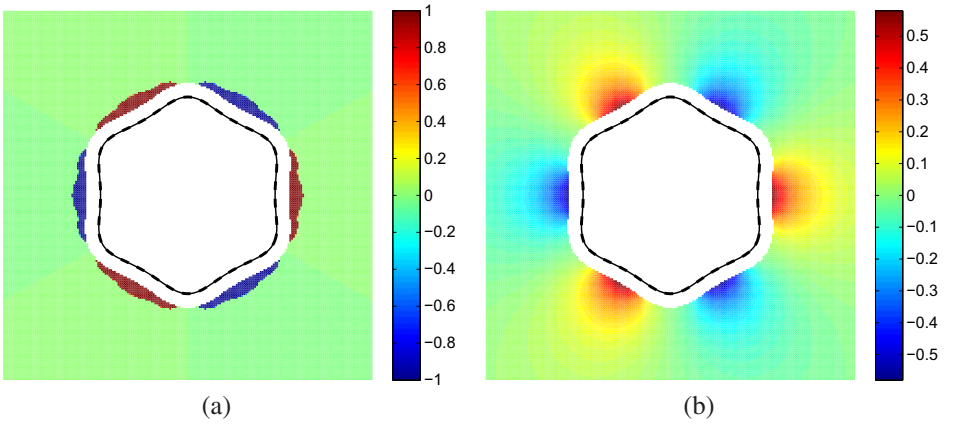

Figure 4. Example 1 – contour plot of $I^{-1} j_0$, (a) penalizing $\|j_0\|_{L_1(\Omega)}$, (b) penalizing $\|j_0\|^2_{L_2(\Omega)}$. Dashed line: target shape, thin solid line: equilibrium shape obtained for the optimized inductors.

several regions with constant $\alpha_p \in \{-1, 0, 1\}$ are clearly identifiable, and the union of these regions is the entire set Θ. In addition, this solution highly reduces the total absolute electric current. The price to pay is a small increment in the Kohn–Vogelius functional from the value 1.34×10^{-11} to 3.50×10^{-10} which produces an imperceptible effect on the equilibrium shape as shown in Figure 2(b). Figure 3 shows the effect of increasing the distance between the inductors and the liquid metal. While in Figure 2(b) the inductors are located to a distance $d = 0.15$ from the liquid metal, in Figure 3(a) $d = 0.25$ and in Figure 3(b) $d = 0.35$, which is almost the distance of the know solution of Figure 1(b). When the distance tends to the value $d = 0.35$, the solutions look more like the known solution, with the total absolute electric current $\psi(j_0) = 0.222$ in the case $d = 0.15$, $\psi(j_0) = 0.274$ for $d = 0.25$ and $\psi(j_0) = 0.349$ for $d = 0.35$, which is still less than the value $\psi(j_0) = 0.384$ of the known solution. The solutions found are then more economical

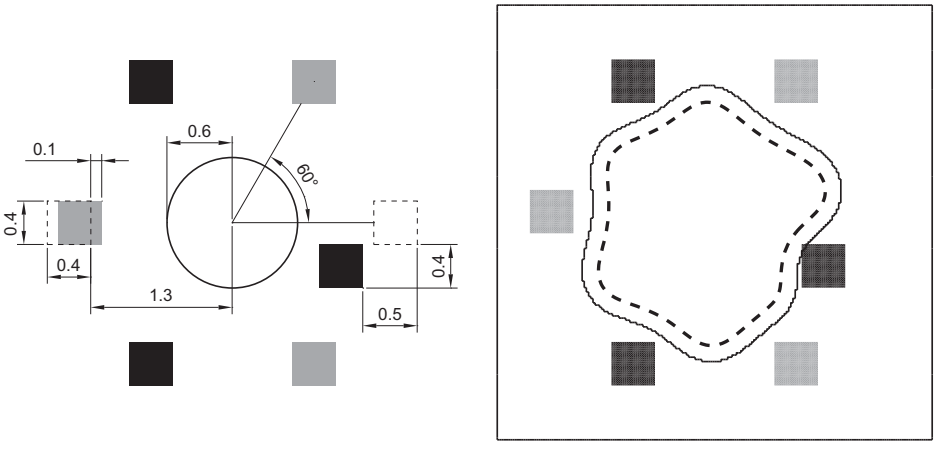

Figure 5. Example 2 – (a) initial configuration of the direct free-surface problem, (b) target shape of area $S_0 = \pi$. Black area: positive inductors, grey area: negative inductors, dashed line: target shape, thin solid line: boundary of the mesh of cells.

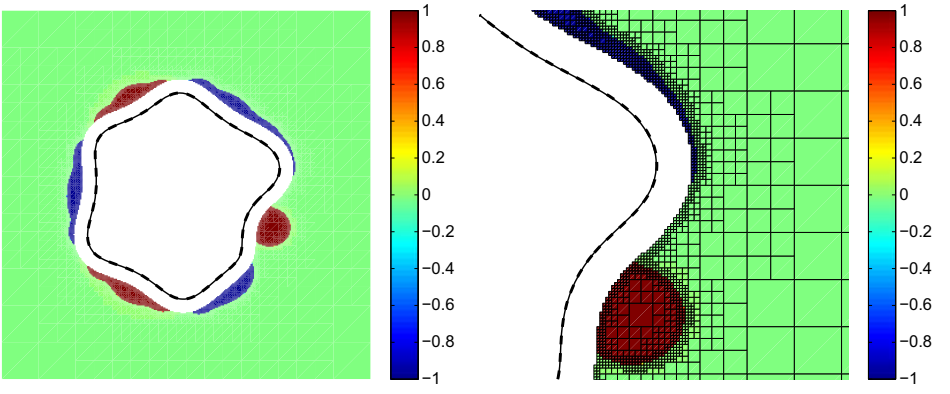

Figure 6. Example 2 – contour plot of $I^{-1} j_0$, (a) solution obtained using a fixed mesh, (b) detail of the solution obtained using a variable mesh. Dashed line: target shape, thin solid line: equilibrium shape obtained for the optimized inductors.

than the known solution, and this fact is due to the addition of the penalty term. Figure 4 shows the importance of choosing an appropriate penalty functional. Figure 4(a) presents the solution obtained by penalizing $\psi(j_0) = \|j_0\|_{L_1(\Omega)}$, while Figure 4(b) shows the solution obtained by penalizing $\|j_0\|^2_{L_2(\Omega)} = \int_\Omega |j_0|^2\, dx$ for a penalty parameter that was chosen to obtain a similar value of the Kohn–Vogelius functional. Note that the second functional leads to a regular solution which is not 0–1. Moreover, the values of the electric current density do not reach the bounds.

In the second example we have moved the inductors of the previous example to generate the asymmetric target shape shown in Figure 5. Note that the initial shape ω in Figure 5(a) does not have the prescribed area $S_0 = \pi$. The algorithm used for solving the direct problem

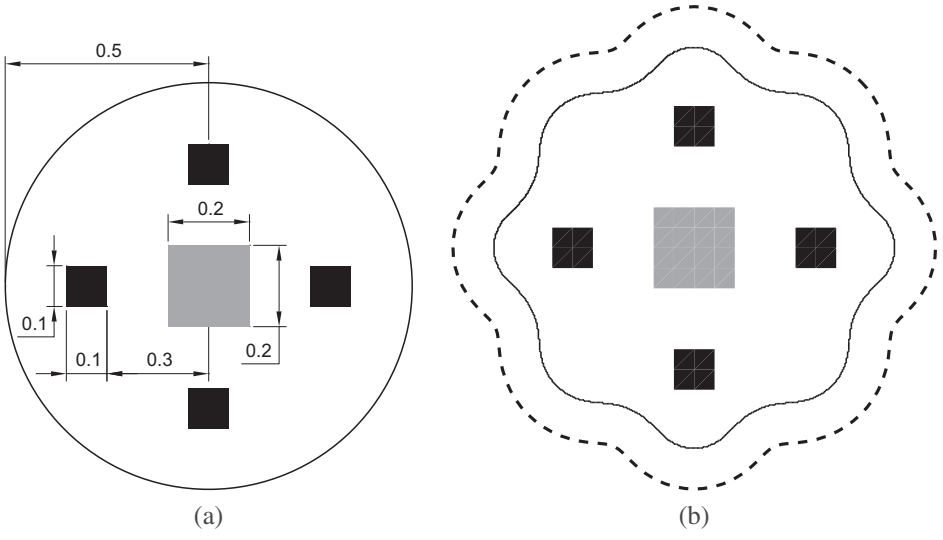

Figure 7. Example 3 – (a) initial configuration of the direct free-surface problem, (b) target shape of area $S_0 = 1$. Black area: positive inductors, grey area: negative inductors, dashed line: target shape, thin solid line: boundary of the mesh of cells.

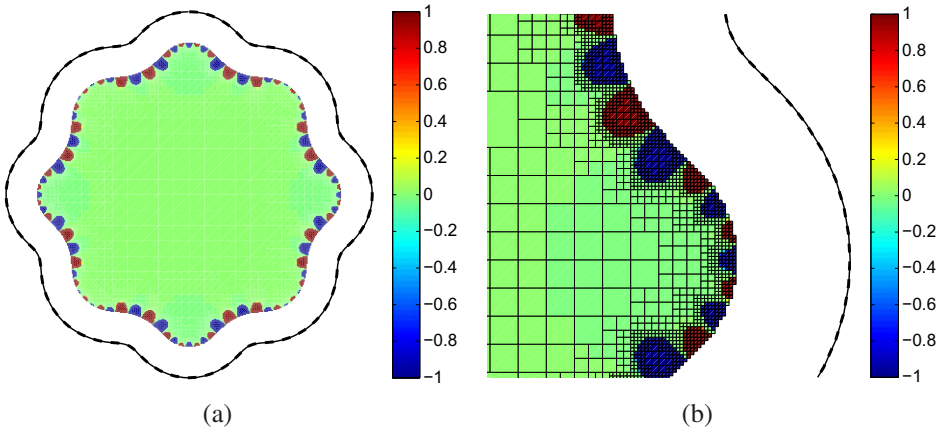

Figure 8. Example 3 – contour plot of $I^{-1} j_0$. Solution obtained using a variable mesh. Dashed line: target shape, thin solid line: equilibrium shape obtained for the optimized inductors.

is a Newton-like iteration applied to a non-linear system containing the area constraint as one of the non-linear equations. Therefore, the algorithm can obtain the correct equilibrium shape, even starting with an infeasible initial ω of area different from S_0; see more details on the area constraint and on the equilibrium and state equations in [1,2]. The inverse problem was solved for $I = 0.4$ and $\rho = 1 \times 10^{-7}$ using both a fixed mesh of cells of size 0.0125 and the variable mesh approach, starting from a mesh of cells of size 0.4 and performing successive mesh refinements until the smallest cells are of size 0.0125. The solutions obtained by both approaches are almost the same, with the difference that the first approach solved a problem of 75433 cells, taking 934 seconds to obtain the solution, while

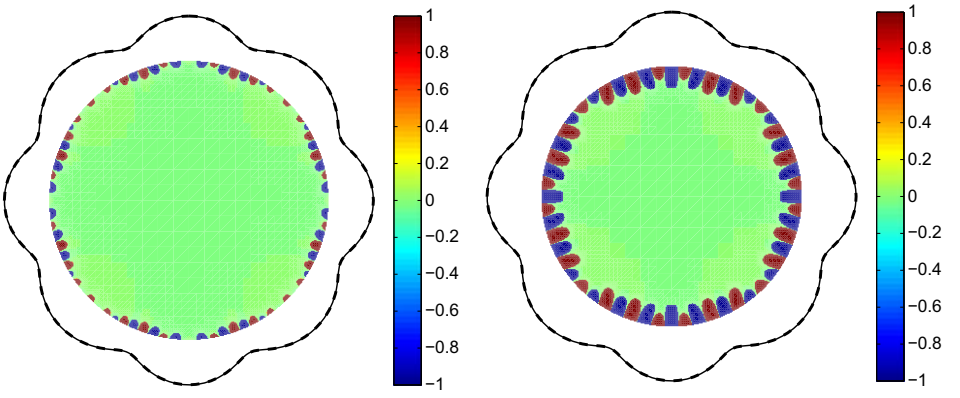

Figure 9. Example 3 – contour plot of $I^{-1}j_0$. Result for a circular Θ of radius (a) $r = 0.45$, (b) $r = 0.42$. Solution obtained using a variable mesh. Dashed line: target shape, thin solid line: equilibrium shape obtained for the optimized inductors.

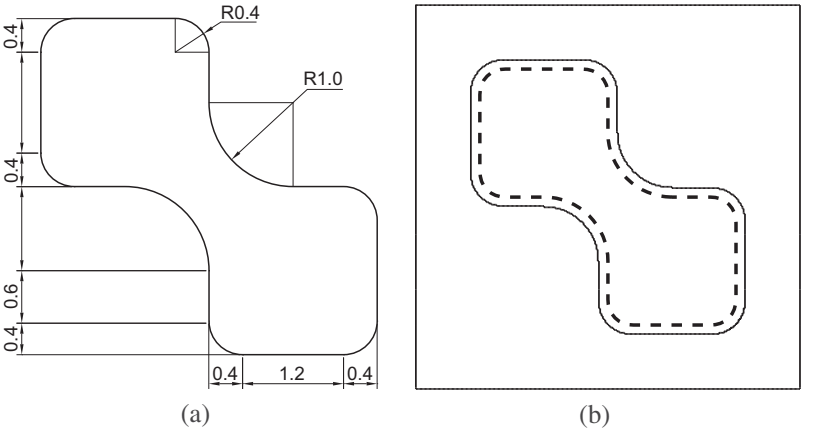

Figure 10. Example 4 – (a) description of the problem geometry, (b) target shape. Dashed line: target shape, thin solid line: boundary of the mesh of cells.

the second approach solved a problem with only 5728 cells in the final mesh, taking only 93 second to solve all the problems from the initial to the final mesh. For this reason, the next examples are all solved using the variable mesh approach. Figure 6 shows the solutions obtained by using the fixed mesh and the variable mesh approach.

The third example corresponds to the equilibrium shape of the interior problem shown in Figure 7. In this case $S_0 = 1.0$, $I = 50.0$ and $\rho = 1 \times 10^{-7}$. The problem was solved by using the variable mesh approach and the solution is shown in Figure 8. This example demonstrates the ability of the current approach to find an economical solution. The solution obtained has a total absolute electric current $\psi(j_0) = 2.784$, while the known solution of Figure 7(a) has $\psi(j_0) = 4.0$. However, unlike the previous exterior problems, the solution j_0 of this interior problem exhibits a spatial pattern of alternating sign. We have seen that the spatial pattern cannot be removed by increasing the penalty parameter ρ, by refining the

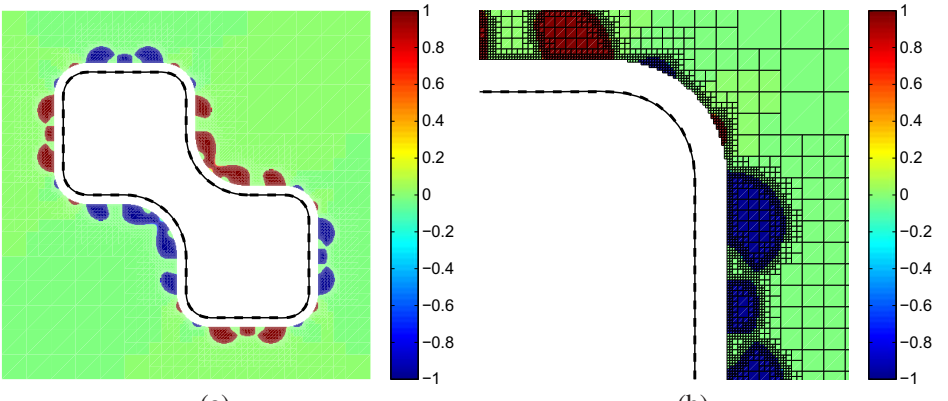

Figure 11. Example 4 – contour plot of $I^{-1} j_0$. Solution obtained using a variable mesh. Dashed line: target shape, thin solid line: equilibrium shape obtained for the optimized inductors.

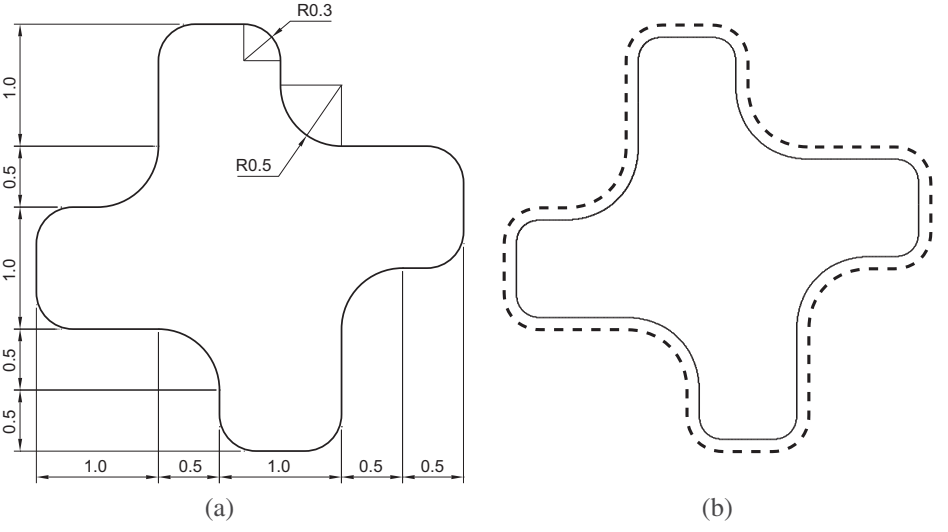

Figure 12. Example 5 – (a) description of the problem geometry, (b) target shape. Dashed line: target shape, thin solid line: boundary of the mesh of cells.

boundary mesh of the liquid metal surface, or by refining the mesh of cells. It also remains if we consider Θ as the circle shown in Figure 9 where we can see that the distance to the liquid metal strongly influences the value of the total absolute electric current which is $\psi(j_0) = 1.875$ in Figure 9(a), and $\psi(j_0) = 6.103$ in Figure 9(b). Further studies should clarify the occurrence of a spatial pattern of alternating sign, which we have not observed in the solution of exterior problems when using the penalty approach.

The fourth and the fifth examples are truly inverse problems defined by target shapes that are not obtained as solutions of direct problems. The fourth example is an exterior problem defined by the target shape depicted in Figure 10, which was also studied in [4].

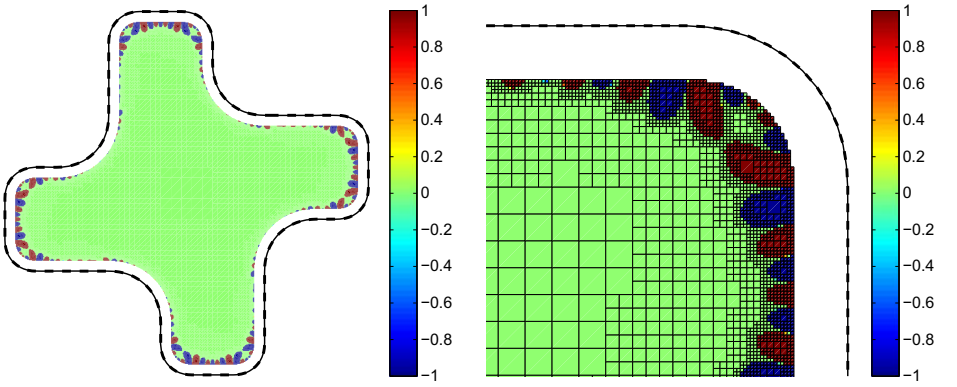

Figure 13. Example 5 – contour plot of $I^{-1} j_0$. Solution obtained using a variable mesh. Dashed line: target shape, thin solid line: equilibrium shape obtained for the optimized inductors.

Table 1. Summary of results.

Example	NMR[a]	Cells[b]	Iterations[b]	Wall time (s)	$J(\phi)$	$\psi(j_0)$
Figure 2(a)	–	29520	21	75.3	1.34×10^{-11}	2.206
Figure 2(b)	–	29520	16	89.4	3.50×10^{-10}	0.222
Figure 3(a)	–	27584	15	93.7	7.13×10^{-10}	0.274
Figure 3(b)	–	25488	19	144.3	6.17×10^{-10}	0.349
Figure 4(b)	–	29520	10	26.0	3.50×10^{-10}	0.405
Figure 6(a)	–	75433	26	934.4	6.37×10^{-10}	0.255
Figure 6(b)	5	5728	28	93.1	6.38×10^{-10}	0.255
Figure 8	5	10072	18	79.0	6.41×10^{-8}	2.786
Figure 9(a)	5	8456	16	66.5	5.87×10^{-8}	1.875
Figure 9(b)	5	13116	24	127.1	1.91×10^{-7}	6.103
Figure 11	5	12307	25	174.5	1.09×10^{-8}	0.375
Figure 13	4	18413	24	364.8	8.07×10^{-8}	1.321

[a]Number of refinements of the mesh of cells.
[b]Number of cells and iterations for the final mesh.

Here, we solved this problem for $I = 0.2$ and $\rho = 1 \times 10^{-7}$, by using the variable mesh approach. Figure 11 shows the solution obtained.

The final example corresponds to the interior problem with the target shape of Figure 12. For $I = 4.0$, $\rho = 1 \times 10^{-7}$ and by using the variable mesh approach, we have obtained the result shown in Figure 13. Note that the solution j_0 exhibits a spatial pattern of alternating sign, which is very similar to the observed in the solutions of the interior problems of Figures 8 and 9.

Table 1 presents a summary of the results obtained for the examples considered.

5. Conclusions

A new topology optimization method for solving an inverse problem concerning the design of the inductors used in EMC has been presented. We have adopted a recently proposed

topology optimization formulation based on the Kohn–Vogelius criterion, and have reformulated it using the SAND approach as an sparse convex quadratic programming problem. The sparse convex quadratic programming nature of the discrete problems allows the use of very efficient interior-point optimization algorithms, and a simple variable mesh approach have been proposed to obtain an additional reduction of the computational costs of solution.

The results presented for some numerical examples show that the addition of an appropriate penalty term, which preserves the quadratic programming structure of the problem, leads to regular 0–1 solutions with a low absolute total electric current. These characteristics indicate that the present approach is optimal for the model considered of the inverse EMC problem.

Acknowledgements

The authors thank the Brazilian Research Councils CAPES, CNPq, FAPERJ, the institutions supporting the programme Ciência Sem Fronteiras of Brazil, the Uruguayan Research Councils ANII and CSIC and the French Research Councils CNRS and INRIA for the financial support.

References

[1] Canelas A, Roche JR, Herskovits J. The inverse electromagnetic shaping problem. Struct. Multidiscip. Optim. 2009;38:389–403.
[2] Canelas A, Roche JR, Herskovits J. Inductor shape optimization for electromagnetic casting. Struct. Multidiscip. Optim. 2009;39:589–606.
[3] Roche JR, Canelas A, Herskovits J. Shape optimization for inverse electromagnetic casting problems. Inverse Probl. Sci. Eng. 2012;20:951–972.
[4] Canelas A, Novotny AA, Roche JR. A new method for inverse electromagnetic casting problems based on the topological derivative. J. Comput. Phys. 2011;230:3570–3588.
[5] Moffatt HK. Magnetostatic equilibria and analogous Euler flows of arbitrarily complex topology. Part 1. Fundamentals. J. Fluid Mech. 1985;159:359–378.
[6] Shercliff JA. Magnetic shaping of molten metal columns. Proc. R. Soc. Lond. A. 1981;375:455–473.
[7] Dulikravich GS, Lynn SR. Unified electro-magneto-fluid dynamics (EMFD): introductory concepts. Int. J. Non-Linear Mech. 1997;32:913–922.
[8] Dulikravich GS, Lynn SR. Unified electro-magneto-fluid dynamics (EMFD): a survey of mathematical models. Int. J. Non-Linear Mech. 1997;32:923–932.
[9] Dennis BH, Dulikravich GS. Magnetic field suppression of melt flow in crystal growth. Int. J. Heat Fluid Flow. 2002;23:269–277.
[10] Dulikravich GS, Colaço MJ. Convective heat transfer control using magnetic and electric fields. J. Enhanc. Heat Transf. 2006;13:139–155.
[11] Colaço MJ, Dulikravich GS. A multilevel hybrid optimization of magnetohydrodynamic problems in double-diffusive fluid flow. J. Phys. Chem. Solids. 2006;67:1965–1972.
[12] Besson O, Bourgeois J, Chevalier PA, Rappaz J, Touzani R. Numerical modelling of electromagnetic casting processes. J. Comput. Phys. 1991;92:482–507.
[13] Sneyd AD. Fluid flow induced by a rapidly alternating or rotating magnetic field. J. Fluid Mech. 1979;92:35–51.
[14] Sneyd AD, Moffatt HK. Fluid dynamical aspects of the levitation-melting process. J. Fluid Mech. 1982;117:45–70.
[15] Jackson JD. Classical electrodynamics. 3rd ed. New York: Wiley; 1998.

[16] Brancher JP, Séro-Guillaume OE. Étude de la déformation d'un liquide magnétique [Study of the deformation of a magnetic liquid]. Arch. Ration. Mech. Anal. 1985;90:57–85.
[17] Gagnoud A, Etay J, Garnier M. Le probléme de frontiére libre en lévitation électromagnétique [The free boundary problem in electromagnetic levitation]. J. Méc. Théor. Appl. 1986;5:911–934.
[18] Henrot A, Pierre M. Un probléme inverse en formage des métaux liquides [An inverse problem in liquid metal forming]. RAIRO Modél. Math. Anal. Numér. 1989;23:155–177.
[19] Novruzi A, Roche JR. Second order derivatives, Newton method, application to shape optimization. Lorraine: NUMATH - INRIA; 1995. (INRIA rapport de recherche; no. RR-2555). Available from: http://hal.inria.fr/inria-00074125/PDF/RR-2555.pdf
[20] Pierre M, Roche JR. Computation of free surfaces in the electromagnetic shaping of liquid metals by optimization algorithms. Euro. J. Mech. B Fluids. 1991;10:489–500.
[21] Pierre M, Roche JR. Numerical simulation of tridimensional electromagnetic shaping of liquid metals. Numer. Math. 1993;65:203–217.
[22] Roche JR. Gradient of the discretized energy method and discretized continuous gradient in electro- magnetic shaping simulation. Appl. Math. Comput. Sci. 1997;7:545–565.
[23] Roche JR. Adaptive Newton-like method for shape optimization. Control Cybern. 2005;34:363–377.
[24] Novruzi A, Roche JR. Newton's method in shape optimisation: a three-dimensional case BIT. Numerical Math. 2000;40:102–120.
[25] Atkinson KE. The numerical solution of integral equations of the second kind, Cambridge monographs on applied and computational mathematics. Vol. 4. Cambridge: Cambridge University Press; 1997.
[26] Nédélec JC. Acoustic and electromagnetic equations. Integral representations for harmonic problems, Applied mathematical sciences. Vol. 144. New York: Springer-Verlag; 2001.
[27] Felici TP, Brancher JP. The inverse shaping problem. Euro. J. Mech. B Fluids. 1991;10:501–512.
[28] Hsiao G, Wendland WL. Boundary integral equations, applied mathematical sciences. Vol. 164. Berlin: Springer-Verlag; 2008.
[29] Canelas A, Herskovits J, Telles JCF. Shape optimization using the boundary element method and a SAND interior point algorithm for constrained optimization. Computers & Structures. 2008;86:1517–1526.
[30] Rozvany GIN. Aims, scope, methods, history and unified terminology of computer-aided topology optimization in structural mechanics. Struct. Multidiscip. Optim. 2001;21:90–108.
[31] Eschenauer HA, Olhoff N. Topology optimization of continuum structures: a review. Appl. Mech. Rev. 2001;54:331–390.
[32] Bendsøe MP. Optimization of structural topology, shape, and material. Berlin: Springer-Verlag; 1995.
[33] Sigmund O, Petersson J. Numerical instabilities in topology optimization: A survey on procedures dealing with checkerboards, mesh-dependencies and local minima. Struct. Optim. 1998;16:68–75.
[34] Sullivan CR. Optimal choice for number of strands in a Litz-Wire transformer winding. IEEE Transac. Power Electron. 1999;14:283–291.
[35] Brebbia CA, Telles JCF, Wrobel LC. Boundary element technique: theory and applications in engineering. Berlin-Heidelberg: Springer-Verlag; 1984.
[36] Brebbia CA, Dominguez J. Boundary elements: an introductory course. Southampton: Second Computational Mechanics Publications; 1992.